Trichoderma reesei Rad51 tolerates mismatches in hybrid meiosis with diverse genome sequences

Wan-Chen Li[a,b,c,1], Chia-Yi Lee[d,1], Wei-Hsuan Lan[e,1], Tai-Ting Woo[c,1], Hou-Cheng Liu[c], Hsin-Yi Yeh[d], Hao-Yen Chang[d], Yu-Chien Chuang[c], Chiung-Ya Chen[c], Chi-Ning Chuang[c], Chia-Ling Chen[c], Yi-Ping Hsueh[c], Hung-Wen Li[e,2], Peter Chi[d,f,2], and Ting-Fang Wang[a,c,2]

[a]Taiwan International Graduate Program in Molecular and Cellular Biology, Academia Sinica, Taipei 11529, Taiwan; [b]Institute of Life Sciences, National Defense Medical Center, Taipei 11490, Taiwan; [c]Institute of Molecular Biology, Academia Sinica, Taipei 11529, Taiwan; [d]Institute of Biochemical Sciences, National Taiwan University, Taipei 10617, Taiwan; [e]Department of Chemistry, National Taiwan University, Taipei 10617, Taiwan; and [f]Institute of Biological Chemistry, Academia Sinica, Taipei 11529, Taiwan

Edited by Scott Keeney, Memorial Sloan Kettering Cancer Center, New York, NY, and approved December 2, 2020 (received for review April 17, 2020)

Most eukaryotes possess two RecA-like recombinases (ubiquitous Rad51 and meiosis-specific Dmc1) to promote interhomolog recombination during meiosis. However, some eukaryotes have lost Dmc1. Given that mammalian and yeast *Saccharomyces cerevisiae* (*Sc*) Dmc1 have been shown to stabilize recombination intermediates containing mismatches better than Rad51, we used the Pezizomycotina filamentous fungus *Trichoderma reesei* to address if and how Rad51-only eukaryotes conduct interhomolog recombination in zygotes with high sequence heterogeneity. We applied multidisciplinary approaches (next- and third-generation sequencing technology, genetics, cytology, bioinformatics, biochemistry, and single-molecule biophysics) to show that *T. reesei* Rad51 (*Tr*Rad51) is indispensable for interhomolog recombination during meiosis and, like *Sc*Dmc1, *Tr*Rad51 possesses better mismatch tolerance than *Sc*Rad51 during homologous recombination. Our results also indicate that the ancestral *Tr*Rad51 evolved to acquire *Sc*Dmc1-like properties by creating multiple structural variations, including via amino acid residues in the L1 and L2 DNA-binding loops.

Trichoderma | homologous recombination | meiosis | Rad51 | Dmc1

Homologous recombination (HR) between maternal and paternal chromosomes is the central theme of meiosis because it generates genetic diversity among haploid gametes and, upon fertilization, among offspring. Meiotic recombination is initiated via programmed double-strand breaks (DSBs), which are preferentially repaired by HR using a homologous nonsister chromosome (interhomolog) rather than a sister chromatid (intersister) as template. Ultimately, the interhomolog DSB repair pathway results in two types of recombination products, cross-overs (COs) and noncross-overs (NCOs). COs involve the exchange of flanking markers and possible gene conversion (GC), whereas NCOs are GC events without exchange of flanking markers. In *Saccharomyces cerevisiae*, the synthesis-dependent strand annealing repair pathway is responsible for the formation of most NCO products, whereas CO products are formed by resolution of Holliday junction intermediates. Chiasma, which are the cytological manifestations of COs, provide a physical link to hold the parental chromosomes together as a bivalent until anaphase I, thereby ensuring proper segregation of parental chromosomes during the first meiotic division (MI) (1–4).

A key step in HR is alignment and pairing of homologous DNAs. The RecA-like recombinases initiate pairing by binding to single-strand DNA (ssDNA) to form a helical nucleoprotein filament. This nucleoprotein filament, often referred to as the presynaptic complex, can pair with double-strand DNA (dsDNA) to yield synaptic complexes consisting of triplex-helical DNA pairing intermediates (5). Sexual eukaryotes fall into two groups with respect to their RecA-like recombinases. The first group (referred to as "dual-RecA eukaryotes") includes budding and fission yeast, higher plants, mammals, and some basidiomycete fungi. The ubiquitous Rad51 (as the only RecA-like enzyme) is responsible for HR during mitosis or vegetative growth in both groups. Rad51 also collaborates with meiosis-specific Dmc1 in the dual-RecA eukaryotes to catalyze interhomolog recombination during meiosis (5). Interestingly, Dmc1 was lost from the second group, which includes *Drosophila melanogaster*, *Caenorhabditis elegans*, and some Pezizomycotina filamentous fungi (e.g., *Neurospora crassa* and *Sodaria macrospora*). It was reported previously that Dmc1 in budding yeast, fission yeast, and mammals is superior to Rad51 in tolerating sequence mismatches during the formation of triplex-helical DNA pairing intermediates (6–10). Consistent with this hypothesis, *S. cerevisiae* Dmc1 (*Sc*Dmc1)-mediated recombination is more efficient than *Sc*Rad51-mediated recombination in highly polymorphic diploid hybrid yeasts (e.g., SK1/S288c and YJM/S288c) (11). The absence of Dmc1 in the "Rad51-only" organisms raises the intriguing question as to how interhomolog recombination is possible among zygotes with highly diversified genome sequences.

Significance

Sexual eukaryotes fall into two groups with respect to their RecA-like recombinases. The first group possesses Rad51 (ubiquitous) and Dmc1 (meiosis-specific), which cooperate to conduct interhomolog recombination in zygotes with high sequence heterogeneity. Interestingly, Dmc1 was lost from the second group of eukaryotic organisms. Here we used the industrial workhorse fungus *Trichoderma reesei* to address if and how Rad51-only eukaryotes carry out hybrid meiosis. We show that *T. reesei* Rad51 (*Tr*Rad51) is indispensable for interhomolog recombination during meiosis and that *Tr*Rad51, like *Saccharomyces cerevisiae* Dmc1, possesses a better mismatch tolerability than *S. cerevisiae* Rad51. Our results indicate that the ancestral *Tr*Rad51 evolved to acquire Dmc1-like properties by adopting multiple structural variations in the L1 and L2 DNA-binding loops.

Author contributions: H.-W.L., P.C., and T.-F.W. designed research; W.-C.L., C.-Y.L., W.-H.L., T.-T.W., H.-C.L., H.-Y.Y., H.-Y.C., C.-L.C., H.-W.L., P.C., and T.-F.W. performed research; W.-C.L., C.-Y.L., W.-H.L., T.-T.W., H.-C.L., C.-Y.C., C.-N.C., Y.-P.H., H.-W.L., P.C., and T.-F.W. contributed new reagents/analytic tools; W.-C.L., C.-Y.L., W.-H.L., T.-T.W., H.-C.L., H.-W.L., P.C., and T.-F.W. analyzed data; and W.-C.L., C.-Y.L., W.-H.L., T.-T.W., H.-W.L., P.C., and T.-F.W. wrote the paper.

The authors declare no competing interest.

This article is a PNAS Direct Submission.

[1]W.-C.L., C.-Y.L., W.-H.L., and T.-T.W. contributed equally to this work.

[2]To whom correspondence may be addressed. Email: hwli@ntu.edu.tw, peterhchi@ntu.edu.tw, or tfwang@gate.sinica.edu.tw.

This article contains supporting information online at https://www.pnas.org/lookup/suppl/doi:10.1073/pnas.2007192118/-/DCSupplemental.

Published February 15, 2021.

Trichoderma reesei, like *N. crassa*, is a Pezizomycotina filamentous fungus. The wild-isolate strain QM6a was originally isolated from one of the Solomon Islands during the Second World War. It is the ancestor of all *T. reesei* workhorse strains currently used for industrial production of lignocellulosic biomass-degrading enzymes and recombinant proteins (12). Sexual mating of *T. reesei*, also like that of *N. crassa*, requires female development, a process by which a female vegetative hypha first forms an ascogonium and then develops into a protoperithecium. The protoperithecium contains a specialized hypha called the trichogyne that is attracted to a male cell, commonly a conidium (the asexual spore), with which it undergoes cell fusion to generate a zygote (13–15). Trichogyne–conidial mating results in maternal transmission of mitochondrial genomes from the female trichogyne parent in these ascomycete fungi. Due to gene mutations in the MAP kinase scaffold protein HAM5 (IDC1) required for female development and vegetative hyphal fusion (anastomosis) (15), the wild isolate QM6a is female sterile. That is why QM6a was thought to be an asexual filamentous fungus for a long time. A milestone in this respect was the finding that QM6a has a *MAT1-2* locus and that it could mate with a female fertile *Hypocrea jacorina* CBS999.97(*MAT1-1*) strain (13). CBS999.97, the teleomorph (sexual reproductive stage) of QM6a, was sampled from French Guiana (16). CBS999.97(*MAT1-1*) and CBS999.97(*MAT1-2*) were derived from two ascospores (i.e., the sexual spores) generated by a CBS999.97 fruiting body, respectively (13). Crosses of CBS999.97(*MAT1-1*) with QM6a or CBS999.97(*MAT1-2*) can induce rapid sexual development under laboratory conditions and generate reproductive structures. The round-shaped stromata (fruiting bodies) are composed of a thallus containing multiple flask-shaped perithecia. Each perithecium contains a bouquet of linear asci (13). The 16 ascospores in each ascus are generated from meiosis, followed by two rounds of postmeiotic mitosis. Accordingly, these 16 ascospores can be divided into four different groups and each group contains four genetically identical ascospores (17).

T. reesei possesses only one copy of a RecA-like recombinase gene (*rad51* but not *dmc1*) (18). In this study, we first show that the genome sequences of QM6a and CBS999.97 possess high sequence heterogeneity. *T. reesei* Rad51 (*Tr*Rad51) proteins are essential for DSB repair during vegetative growth, as well as for interhomolog recombination during meiosis. We also report that *Tr*Rad51, like *Sc*Dmc1 but not *Sc*Rad51, can stabilize mismatches during the formation of triplex-helical DNA pairing intermediates, thereby promoting interhomolog recombination during hybrid meiosis of QM6a and CBS999.97(*MAT1-1*).

Results

Highest-Quality Genome Sequences Yet of CBS999.97(*MAT1-1*) and CBS999.97(*MAT1-2*). The near-complete genome sequence of QM6a was determined using both next-generation sequencing (NGS) and third-generation sequencing (TGS) technology (18). Here, we applied the same methods to sequence and assemble the genome sequences of CBS999.97(*MAT1-1*) and CBS999.97(*MAT1-2*) (*SI Appendix*, Tables S1 and S2). Like QM6a (18), CBS999.97(*MAT1-1*) and CBS999.97(*MAT1-2*) have eight reference chromosomes (seven nuclear chromosomes plus a circular mitochondrial DNA). Of these, all seven nuclear chromosomes were essentially returned as seven single, complete unitigs, respectively (*SI Appendix*, Fig. S1*A*). We confirmed a reciprocal translocation event in CBS999.97(*MAT1-1*) (*SI Appendix*, Fig. S1 *A* and *B*) by pulsed-field gel electrophoresis and Southern hybridization (*SI Appendix*, Fig. S1 *C–F*) (17). Except for the left terminus of chromosome VI (i.e., due to incomplete genome sequence and assembly), all other chromosomal ends in CBS999.97(*MAT1-1*) and CBS999.97(*MAT1-2*) contain 8 to 13 telomeric repeats (i.e., TTAGGG at 3′ termini and the reverse complement CCCTAA at 5′ termini) (18) (*SI Appendix*, Table S3).

Three lines of evidence confirm the high quality of these three genome sequences. First, their Phred quality scores ($Q \equiv -10 \times \log_{10}P$) are 48.8 (QM6a), 48.1 [CBS999.97(*MAT1-1*)], and 48.7 [CBS999.97(*MAT1-2*)]. Q is logarithmically linked to in probability of incorrect base call (P). For example, if Q = 50, the chance of error probability is 1 in 100,000 (19). Second, the OrthoDB-based BUSCO software program was also used to quantitatively measure the completeness of genome assembly. BUSCO is an open-source software with a large selection of lineage-specific sets of Benchmarking Universal Single-Copy Orthologs (20, 21). OrthoDB presents a catalog of orthologous protein-encoding genes across vertebrates, arthropods, fungi, plants, and bacteria (22). It was reported that model organisms, which have good reference genomes, often reach a genome or protein matric (score) above 95% complete (21). The BUSCO genome metrics of QM6a, CBS999.97(*MAT1-1*), and CBS999.97(*MAT1-2*) are 100.0%, 98.5%, and 98.4% complete, respectively. We also applied *Funannotate* as a fungal genome annotation script (23) for genome reannotation. Their BUSCO protein metrics are 96.8%, 98.8%, and 98.3% complete, respectively (*SI Appendix*, Table S2).

Due to the occurrence of repeat-induced point mutation (RIP) in *T. reesei* (18), both CBS999.97 haploid genome sequences contain only 62 transposable elements (*SI Appendix*, Table S4) but harbor 2249 AT-rich blocks with length ≥500 base pairs (bp) (*SI Appendix*, Table S5). RIP, a genome-defense mechanism conserved in many Pezizomycotina fungi, occurs premeiotically in haploid parental nuclei in preparation for karyogamy and meiosis. It detects duplications of chromosomal DNA above a certain length threshold (~400 bp), leading to cytosine-to-thymine (C-to-T) mutation and concomitant methylation in a pairwise fashion on both strands of each DNA duplex (24–26). It is important to note that these AT-rich blocks might have important functions in fungal–plant interactions, symbiosis, genome evolution (e.g., gene loss, duplication, and neofunctionalization), or genome organization and transcription (18, 27, 28). Thus, it is crucial to determine if sexual development and meiotic recombination exert any influence on these AT-rich blocks.

QM6a and CBS999.97 Exhibit High Levels of Sequence Heterogeneity. High-quality genome sequences allow efficient variant calling for genetic and genomic studies. We applied two different approaches to identify single-nucleotide polymorphisms (SNPs) and insertion/deletion mutations (InDels). For convenience, to perform telomere-to-telomere sequence alignment between two homologous chromosomes in a hybrid diploid cell (discussed below), InDels can be converted into SNPs by filling in the null (n) or (−) spaces. Accordingly, we collectively refer to SNPs and InDels as allelic point disparities (APDs). It is important to note that an SNP is a nucleotide polymorphism between two homologous sequences that otherwise align. In contrast, APDs are single-nucleotide disparities between the allelic sequences of two homologous chromosomes, though one of the two allelic sequences might contain only (n) spaces due to insertion or deletion.

MUMmer4, a high-stringency variant detection pipeline (29), called out 935,999 APDs between QM6a and CBS999.97(*MAT1-1*) (*SI Appendix*, Table S6), 949,448 APDs between QM6a and CBS999.97(*MAT1-2*) (*SI Appendix*, Table S7), and 2,705 APDs between CBS999.97(*MAT1-1*) and CBS999.97(*MAT1-2*) (*SI Appendix*, Table S8). These APDs are distributed quite evenly between the seven chromosomes of QM6a and CBS999.97(*MAT1-1*) (*SI Appendix*, Fig. S2). In order to investigate genome-wide patterns of meiotic recombination in *T. reesei*, a hybrid strain similar to it is necessary, as has been performed previously for budding yeast (11). Thus, sexual crossing of QM6a and CBS999.97(*MAT1-1*) is an ideal experimental model for our study.

There is a pitfall to utilizing MUMmer4 or other NGS-based software tools for variant calling. These software tools ignored the most "difficult-to-align" nucleotide sequences between the two wild isolates. Almost all identified APDs are not located in highly heterologous regions. This is particularly true for InDels of length ≥50 bp (30). Our results reveal that the longest continuous InDel detected by MUMmer4 is 86 bp in length (Dataset S1, Table D1B), raising concerns about the lack of sufficient APDs for revealing interhomolog recombination products and/or other sequence variations within those "difficult-to-align" DNA sequences. Consequently, we also conducted this analysis using TSETA (TGS to Enable Tetrad Analysis), a new pipeline that utilizes chromosome-level sequence assembly for "telomere-to-telomere" variant calling via multiple genome sequence alignment (MGSA) (31). Using the "SNP" mode of TSETA for variant calling, we found that TSETA was about ≥6.5 times more powerful than MUMmer4 (6,157,980 APDs vs. 935,999 APDs, respectively) in revealing sequence diversity between QM6a and CBS999.97(*MAT1-1*) (*SI Appendix*, Table S6). In general, TSETA detected higher overall numbers of SNPs and InDels and also longer continuous InDels (Dataset S1, Tables D1A and D1B). The longest continuous InDel detected by TSETA is 61,695 bp in length (Dataset S1, Table D1B). Intriguingly, our results also reveal that, due to employing different sequence alignment algorithms, MUMmer4 revealed much more singlet or short InDels (of only 1 to 3 bp) than TSETA (Dataset S1, Table D1B) during the process of comparing similarity between the two allelic sequences. Accordingly, only MUMmer4, but not TSETA, introduced three (*SI Appendix*, Fig. S3*A*) and two (*SI Appendix*, Fig. S3*B*) short sequence discontinuities or gaps in two representative low-complexity regions, respectively. Presumably, some of these short gaps introduced by MUMmer4 (e.g., *SI Appendix*, Fig. S3*A*) may have impeded genome-wide mapping of meiotic recombination products using classical NGS short reads (discussed below).

For simplicity, we only consider longer continuous InDels (>86 bp) revealed by TSETA as "unalignable" sequences because the longest continuous InDels revealed by MUMmer4 are 86 bp in length (Dataset S1, Table D1B). Since the overall length of the QM6a genome is 34,139,199 bp, we estimate sequence heterogeneity between these two isolates to be ∼18.04%, ∼4.77%, and ∼3.34% when all APDs, all SNPs plus the alignable InDels (i.e., continuous InDels of ≤86 bp), and only all SNPs are considered as "strain-specific" sequences, respectively.

Genome-Wide Detection of Meiotic Recombination Products with Single-Nucleotide Precision. Next, we applied two different methods to reveal genome-wide meiotic recombination profiles. The first method utilized 1) all APDs revealed by MUMmer4 and 2) classical NGS short sequencing reads to genotype APD positions among four representative F1 progeny relative to either one of the two parental genomes [QM6a or CBS999.97(*MAT1-1*); *Materials and Methods*]. The results were then analyzed in two publicly available programs [ReCombine (v2.1) (32) and GroupEvents programs (33)] to detect CO and NCO products. To assess efficacy, we first used this pipeline to reanalyze the NGS data on budding yeast tetrads from wild-type (WT) SK1/S288c (11, 34, 35) and *dmc1*Δ *hed1*Δ SK1/S288c hybrid meiosis (11). Hed1 is a meiosis-specific inhibitor of Rad51. The genomes of S288c and SK1 contain 12,157,149 bp and 12,063,285 bp, respectively. MUMmer4 called out 100,109 APDs (78,337 SNPs and 21,772 InDels), whereas TSETA revealed 1,157,584 APDs (212,640 SNPs and 944,944 InDels) between these two yeast strains (Dataset S1, Tables D2A and D2B), respectively. The longest continuous InDels detected by MUMmer4 and TSETA are 81 bp and 28,190 bp, respectively (Dataset S1, Table D2B). From the variant calling results revealed by TSETA, we estimate the sequence heterogeneity between these two isolates to be ∼9.59%, ∼2.21% [(212,640 + 56,267)/12,157,149)] and ∼1.75%, when all APDs, all SNPs and the alignable InDels (i.e., continuous InDels of ≤81 bp), or only all SNPs are considered as "strain-specific" sequences, respectively. These results indicate that the ratios of both alignable and unalignable sequence variations between S288c and SK1 are lower than those between QM6a and CBS999.97(*MAT1-1*). Thus, a naïve expectation would be that *Tr*Rad51 should be more tolerant to mismatches than *Sc*Rad51 in the process of catalyzing interhomolog recombination during meiosis.

We were able to detect all of the CO and NCO (with at least two consecutive 3:1 and/or 4:0 markers) products reported previously (11). We then determined the genome-wide meiotic recombination landscapes of three asci (#1–#3) generated by QM6a and CBS999.97(*MAT1-1*) hybrid meiosis (Table 1 and *SI Appendix*, Table S9). All 48 ascospores from these three asci could germinate and formed mycelia with dark-green conidial pigments, indicating that they are all euploid (17). The genomic DNA of the 48 F1 progeny was isolated and genotyped to detect *mat1-1*, *mat1-2*, and *actin*, as described previously (17). The PCR results revealed that the 16 ascospores in each ascus can be classified into four genetically identical groups (17, 18). One representative ascospore from each genetically identical group was then selected for whole-genome sequencing using an Illumina-Nextseq sequencer. We then used PlotTetrad, a component of the "ReCombine" programs (32), to create graphical

Table 1. Summary of CO and NCO products in the three asci generated by sexual crossing of QM6a with CBS999.97(*MAT1-1*)

	Chromosome							
	I	II	III	IV	V	VI	VII	I–VII
Ascus #1 (TSETA)*								
RIP (Q)†	334	61	19	867	71	1,478	243	3,073
RIP (C)‡	12	15	12	17	5	14	17	92
CO	2	1	1	1	1	1	1	8
CO w/GC	3	2	2	2	3	2	2	16
NCO§	1	1	4	1§	2	1	0	10
Total	24 COs and 10 NCOs§							
Asci #1 (NGS)¶								
CO	2	1	1	1	1	1	1	8
CO w/GC	3	2	2	2	3	2	2	16
NCO	1	1	4	0	2	1	0	9
Total	24 COs and 9 NCOs							
Ascus #2 (NGS)¶								
CO	2	1	2	1	2	0	1	9
CO w/GC	3	3	2	2	1	2	2	15
NCO	3	3	3	2	0	1	1	13
Total	24 COs and 13 NCOs							
Ascus #3 (NGS)¶								
CO	1	2	2	2	1	0	0	8
CO w/GC	3	4	1	2	3	4	2	19
NCO	2	4	3	0	1	2	3	15
Total	27 COs and 15 NCOs							

*The genomic DNA of four representative F1 progeny was determined by PacBio SMRT technology and analyzed by TSETA to identify genome-wide meiotic recombination events.

†The number of RIP mutations occurring between two QM6a sister chromatids.

‡The number of RIP mutations occurring between two CBS999.97(MAT1-1) sister chromatids.

§TSETA not only detects all CO and NCO interhomolog products revealed by the NGS-based method but also one additional authentic NCO products in the #1 ascus (*SI Appendix*, Table S10).

¶The genomic DNA of four representative F1 progeny was determined by an Illumina-NextSeq sequencer and analyzed by MUMmer4 to identify genome-wide meiotic recombination events.

representations of all seven chromosomes of QM6a and CBS999.97(*MAT1-1*), as well as the four representative progeny from each ascus (*SI Appendix*, Fig. S4). We found that all the interhomolog recombination products in these three *T. reesei* asci (#1–#3) are "simple COs" or "simple NCOs," without any other genotype switches within 5 kb (Table 1 and *SI Appendix*, Table S9). This feature differs from budding yeast meiosis, which often generates COs with discontinuous GC, NCOs with two GC tracts, or even ambiguous recombination products that can arise from more than one pathway (32).

There are two technical concerns in applying the NGS-based approach to detect genome-wide meiotic recombination products. First, due to the short lengths of Illumina paired-end reads, it is technically challenging to correctly map the NGS short reads to the genome sequences in low-complexity regions with repetitive and long AT-rich sequences (18). Thus, almost all NGS short reads with low sequence complexity are filtered out for sequence mapping. Second, as described above, superfluous "short sequence gaps" introduced by MUMmer4 (*SI Appendix*, Fig. S3) can impede accurate mapping of classical NGS short reads (*SI Appendix*, Fig. S5). To overcome this issue, we also applied PacBio SMRT (single molecule real-time) technology (31, 36) to sequence and assemble the complete genomes of the four representative F1 progeny in ascus #1 (*SI Appendix*, Table S1). Next, TSETA was used again to accurately map and visualize genome-wide meiotic recombination products (Fig. 1*B*). We found that TSETA not only could detect all CO and NCO products revealed by the NGS-based approach but it also outcompeted the latter by identifying one more authentic NCO product in the first ascus (Table 1, *SI Appendix*, Table S10, and Dataset S2). The classical NGS-based mapping method we used here failed to map and determine the corresponding sequences in the four representative F1 progeny (*SI Appendix*, Fig. S5). A close examination revealed that the nucleotide sequences involved in this authentic NCO harbor a longer polyA/T fragment in QM6a and a shorter polyA/T fragment in CBS999.97(*MAT1-1*) (*SI Appendix*, Figs. S3 and S5).

TSETA is a powerful MGSA tool since it also allows detection of genome-wide RIP events (Table 1), illegitimate mutations (IMs), and illegitimate deletions (IDs) (Fig. 1*B*) generated in the same meiosis event (31). IMs represent positions where ≥1 F1 progeny harbor an authentic nucleotide but the corresponding

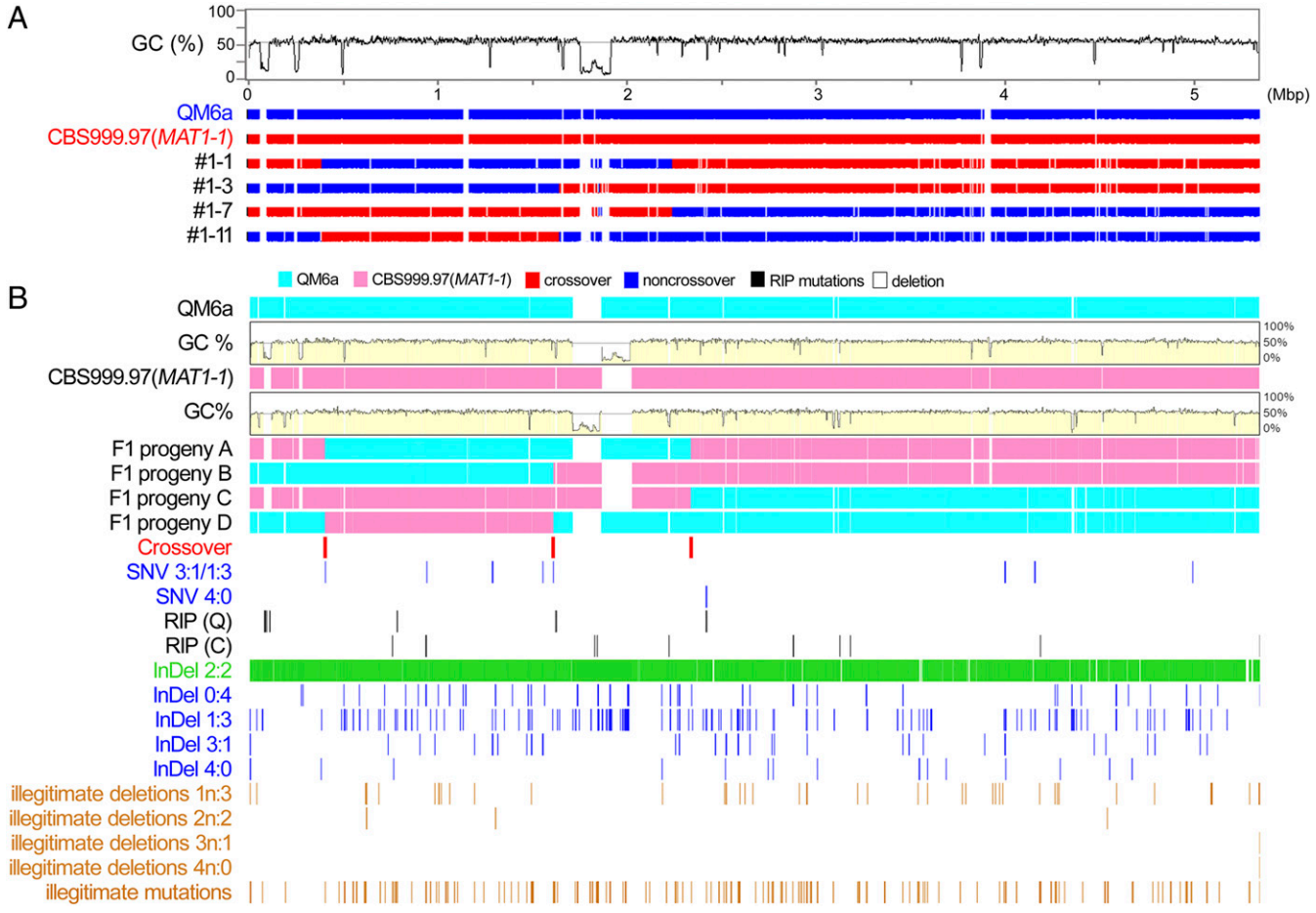

Fig. 1. *T. reesei* QM6a/CBS999.97(*MAT1-1*) hybrid meiosis generates interhomolog recombination products. (*A*) NGS-based mapping of meiotic recombination products. The first trace represents a graph of GC content (window size 5,000 bp) for the telomere-to-telomere sequence of the first QM6a chromosome. Nucleotide sequences of QM6a (in blue), CBS999.97(*MAT1-1*) (in red) and the four representative F1 progeny are shown. Due to the short lengths of NGS reads, it is difficult to accurately assemble the nucleotide sequences of chromosome regions (in white) hosting repetitive and/or high AT-biased sequences. (*B*) TGS-based mapping of meiotic recombination products using the newly developed software program TSETA (31). The first two horizontal rows of sequence data represent the full-length sequences of the third chromosomes (ChIII) of QM6a (in cyan) and CBS999.97(*MAT1-1*) (in magenta). The next four horizontal rows of sequence data represent full-length ChIII of the four representative F1 progeny, respectively. Nucleotide sequences identical to those of parental QM6a and CBS999.97(*MAT1-1*) are also indicated in cyan and magenta, respectively. COs are located where 2:2 markers undergo a reciprocal genotype change. The strain-specific or gapped (deletion) regions are colored white. The positions of COs, 0:4, 1:3, 3:1, and 4:0 SNP or InDel markers, as well as RIP mutations, IMs, and IDs (i.e., 1n:3, 2n:2, 3n:1, or 4n:0 segregation markers) are indicated by vertical lines (31).

nucleotides in one or both parental genomes are null (n). In contrast, IDs are gapped positions with authentic nucleotides in both QM6a and CBS999.97(*MAT1-1*), but the corresponding positions in the four F1 progeny show 1n:3, 2n:2, 3n:1, or 4n:0 segregation, where 1n, 2n, 3n, and 4n represent the numbers of F1 progeny with a null (−) at a selected nucleotide position (Fig. 1*B*). We found that more RIP events occur in QM6a (3,073 nucleotides) than in CBS999.97(*MAT1-1*) (92 nucleotides) (Table 1 and Fig. 1*B*). This finding is not too surprising for two reasons. First, the CBS999.97(*MAT1-1*) strain we used was previously derived from an ascospore of *H. jecorina* fruiting body (13), indicating that its genome had undergone previously one or more rounds of RIP. Second, QM6a is female sterile and has been propagated vegetatively for ≥70 y. Accordingly, the genome of QM6a has accumulated more repetitive sequences and transposable elements than that of CBS999.97(*MAT1-1*) (*SI Appendix*, Table S4).

DNA Replication Error Rates during the Two Rounds of Postmeiotic Mitosis and Postgermination Growth. To rule out the possibility that unexpected variations or even interhomolog recombination products might be generated during two rounds of postmeiotic mitosis, we also sequenced the genomic DNA from all 16 F1 progeny generated from the #1 asci using an Illumina-Nextseq sequencer (*SI Appendix*, Table S1). To do that, we used the near-complete and high-quality PacBio genome sequences of four representative F1 progeny (i.e., #1–1, #1–3, #1–7, and #1–11; Fig. 1*B* and *SI Appendix*, Table S1) as templates to assemble the four NGS-based genome sequences in each genetically identical group (*Materials and Methods*). The overall error rates of these four PacBio F1 genomes were extremely low [<0.0007% = 1/(39,004 × 4) × 100%], as the nucleotide sequences of their mitochondrial genomes were not only completely identical to each other, but they also contained only six SNPs (i.e., three 1-bp deletions and three 1-bp insertions) relative to that of the CBS999.97(*MAT1-1*) mitochondrial genome (*SI Appendix*, Table S11). Interestingly, the CBS999.97(*MAT1-1*) mitochondrial genome (39,004 bp) only shares 75% identity in nucleotide sequence with that of QM6a (42,139 bp). Although there are SNPs (1,357 bp) and InDels (10,917 bp) between these two mitochondrial genomes, each encodes the same set of genes essential for mitochondrial functions, including ATP production, electron transport, and translation of mitochondrial proteins (*SI Appendix*, Table S12). These results are consistent with the notion that QM6a is female sterile (13) and that all mitochondria in the F1 progeny are inherited maternally from CBS999.97(*MAT1-1*).

Next, we conducted pairwise sequence alignment and comparisons using the SNP mode of TSETA to identify SNPs and InDels between the 16 F1 NGS-based genome sequences. We found very few SNPs (8 to 42 bp) or InDels (42 to 373 bp) between the four genome sequences in each genetically identical group. In contrast, we identified many SNPs (500,000 to 720,000 bp) and InDels (1,800,000 to 4,500,000 bp) between any two F1 genomes from different groups (*SI Appendix*, Table S13). Accordingly, these results indicate that the error rate of DNA replication during two rounds of postmeiotic mitosis and postgermination growth is <0.0002% [i.e., (42 + 373)/34,139,199 × 100%], which is about 3.5-fold lower than that (<0.0007%) of the PacBio RSII sequencing platform (with >80-fold sequencing coverage), as described above. Although these results support the notion that the majority of the sequence variations we detected in the four representative F1 progeny were generated during meiosis rather than during two rounds of postmeiotic mitosis, it is noteworthy that mutation rates caused by DNA replication, mostly in bacteria, have been reported to be as low as 10^{-8} to 10^{-9} (37).

SNPs in the GC Tracts of Interhomolog Recombination Products. The NGS-based variant calling method identified 75 CO and 37 NCO products in the three QM6a/CBS999.97(*MAT1-1*) asci (Table 1). Next, we further assessed the APDs revealed by TSETA (*SI Appendix*, Table S6) to determine APD number and the length of GC tracts associated with all interhomolog products. Compared to the median GC length (~1,000 bp) of SK1/S288c hybrid meiosis (11), *T. reesei* WT meiosis generated COs and NCOs with much shorter median GC lengths (200 to 250 bp) (Fig. 2*A*, *SI Appendix*, Table S14, and Dataset S2).

The median APD density per CO product (i.e., the number of APDs vs. the length of GC tracts) in QM6a/CBS999.97(*MAT1-1*) hybrid meiosis is 17.5 APDs per 1,000 bp, which is ≥3.6-fold higher than that of WT SK1/S288c hybrid meiosis (4.8 APDs per 1,000 bp) and SK1/S288c *dmc1*Δ *hed1*Δ hybrid meiosis (4.7 APDs per 1,000 bp) (Fig. 3*B* and *SI Appendix*, Table S15). Intriguingly, we identified several long GC tracts containing a large number of APDs (up to 50) in QM6a/CBS999.97(*MAT1-1*) hybrid meiosis (Fig. 2*B* and *SI Appendix*, Table S15). Since *T. reesei* possesses relatively low DNA replication error rates (<0.0002%), one potential explanation for this observation is that the RecA-like recombinase in *T. reesei* can tolerate mismatched sequences during the formation of triplex-helical DNA pairing intermediates.

***T. reesei* Is a Rad51-Only Eukaryote.** The *T. reesei* genome encodes one RecA-like recombinase (i.e., *Tr*Rad51) and the Rad51-specific accessory factors (*Tr*Rad52, *Tr*Rad54, *Tr*Rad55, and *Tr*Rad57), but not Dmc1 or any Dmc1-specific accessory factors (Hop2, Mnd1, Mei5, or Sae3) (18). The chromosomal locations of *Tr*Rad51 and the Rad51-specific accessory factors (*Tr*Rad52, *Tr*Rad54, *Tr*Rad55, and *Tr*Rad57) in the genome sequences of QM6a, CBS999.97(*MAT1-1*), and CBS999.97(*MAT1-2*) are provided (*SI Appendix*, Table S16). The conserved primary structures and well-aligned protein sequences with other fungal orthologs strongly support our identification of these important HR-related proteins in *T. reesei* (*SI Appendix*, Figs. S6–S10). Phylogenetic analysis further confirmed that the amino acid sequences of all Rad51 proteins (i.e., from both "dual-RecA" and "Rad51-only" eukaryotes) share higher identity or homology with each other than those of Dmc1 proteins (*SI Appendix*, Fig. S11). Accordingly, we were interested in determining if *Tr*Rad51 can mediate interhomolog recombination in the QM6a/CBS999.97 hybrid zygotes.

***T. reesei rad51* Is Indispensable for DNA Damage Repair during Normal Vegetative Growth and Meiosis.** Next, we generated two *rad51*Δ mutants by HR-based gene replacement and then confirmed gene deletion by Southern hybridization (Fig. 3*A*). *Tr*Rad51 proteins were heterologously expressed and purified in *Escherichia coli* (discussed below) (38) and then used to generate mouse monoclonal antibodies (*Materials and Methods*). The vegetative mycelia of WT QM6a and the *rad51*Δ mutants were harvested for preparation of total cell lysates using the trichloroacetic acid precipitation protocol described previously (39). The results of immunoblotting analysis confirmed that *Tr*Rad51 was present only in WT mycelia but not in *rad51*Δ mycelia (Fig. 3*B*).

We then determined if *Tr*Rad51 is essential for DNA damage repair during vegetative growth. The conidia (i.e., asexual spores) of WT and four different mutants (*rad51*Δ, *mus53*Δ, *ku70*Δ, and *mus53*Δ *ku70*Δ) were subjected to spot assays with fivefold serial dilutions on malt extract agar (MEA) plates containing no or 0.015% (wt/vol) of the DNA damage agent methyl methanesulfonate (MMS). *ku70* and *mus53* encode the nonhomologous end-joining DNA repair protein Ku70 and DNA ligase IV (Lig4), respectively (40, 41). We found that only *rad51*Δ, but

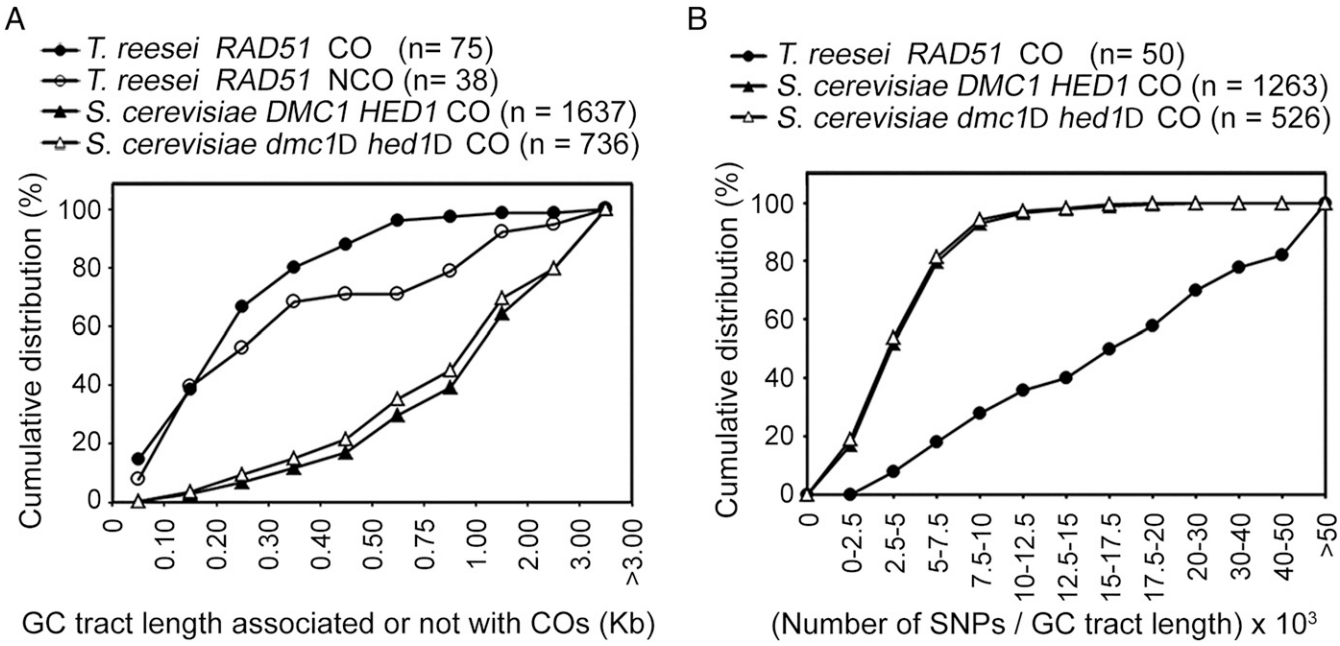

Fig. 2. Comparative analysis of all COs and NCOs in the three QM6a/CBS999.97(*MAT1-1*) hybrid asci. The NGS results of 23 different SK1/S288c tetrads published previously (11) were reanalyzed here. (*A*) Cumulative distribution of the GC lengths associated with CO and/or NCO during hybrid meiosis of QM6a/CBS999.97(*MAT1-1*) and SK1/S288c. TSETA detected 1,715 putative NCO products (with one or more 0:4, 1:3, 3:1, or 4:0 markers) in the first asci (Dataset S2). However, the majority of these are "false-positive" NCOs due to either RIP or InDels associated with poly-A/T or poly-G/C low-complexity regions. Accordingly, only NCOs with ≥2 APDs (i.e., the sum of SNPs + InDels) and ≥1 SNP are analyzed here (*SI Appendix*, Table S14). (*B*) Cumulative distribution of APD density in the CO-associated GC tracts is shown. Two-sample Kolmogorov–Smirnov tests (two-sided) confirmed that both cumulative distributions are significantly different (***$P < 0.001$).

not *mus53*Δ, *ku70*Δ, or *mus53*Δ *ku70*Δ, exhibited slow vegetative growth in the presence of 0.015% MMS (Fig. 3*C*).

We also observed that deletion of *rad51* resulted in no apparent effect on formation of fruiting bodies, perithecia (Fig. 3*D*), and asci (Fig. 3*E*). WT fruiting bodies produced mature asci with 16 ascospores 5 to 7 d after mating QM6a with CBS999.97(*MAT1-1*). In contrast, the majority of *rad51*Δ asci (>65%; $n = 100$ from five different fruiting bodies) were arrested at meiotic prophase and possessed only one nucleus even 10 d after mating QM6a *rad51*Δ with CBS999.97(*MAT1-1*) *rad51*Δ. Approximately one-third of the *rad51*Δ asci advanced to MI and/or MII, but none of these asci underwent sporulation and formed ascospores (Fig. 3*F*).

These results reveal that *Tr*Rad51 is not only required for MMS-induced DNA damage repair during mitosis but also for HR between parental homologous chromosomes during meiosis.

***Tr*Rad51 Exhibits a Better Mismatch Tolerance for DNA Strand Exchange.** We then expressed, purified, and biochemically characterized *Tr*Rad51. Our results revealed that *Tr*Rad51 possesses the universal features of recombinases (*SI Appendix*, Figs. S12–S15). Like *Sc*Dmc1, *Tr*Rad51-mediated strand exchange activity is enhanced by Ca^{2+} (*SI Appendix*, Fig. S16). Next, we employed a fluorescence-based strand exchange assay (42) to monitor the process in real time. Upon strand exchange, two cyanine dyes (Cyanaine 3, Cy3 and Cyanine 5, Cy5) labeled on each strand of homologous duplex DNA separate. Consequently, fluorescence emission of Cy3 cannot be efficiently transferred to Cy5, resulting in increased Cy3 fluorescence (Fig. 4*A*). In addition to homologous substrate, we also designed mismatched substrate in which one mismatched nucleotide was located at the center of the ssDNA (Fig. 4*B*). A similarly designed mismatched base pair was previously documented to differentiate the mismatch tolerance of the *Sc*Rad51 and *Sc*Dmc1 recombinases in single-molecule analyses (7, 10). To carry out fluorescence-based strand exchange, we incubated purified recombinases (*Sc*Dmc1, *Sc*Rad51, or *Tr*Rad51) (*SI Appendix*, Figs. S12*C* and S15) with either homologous or mismatched ssDNA to assemble nucleoprotein filament. Next, the fluorophore-labeled dsDNA was included in the reaction to initiate the strand-exchange process. As shown in Fig. 4, both *Sc*Rad51 and *Sc*Dmc1 conducted DNA strand exchange with homologous substrate (Fig. 4*C*). Importantly, the one mismatched base pair impaired by about 50% the strand exchange ability of *Sc*Rad51, but not that of *Sc*Dmc1. Thus, our fluorescence-based strand-exchange assay allows us to measure DNA strand exchange in real-time and to differentiate the mismatch tolerance ability of recombinases.

*Tr*Rad51 can efficiently carry out DNA strand exchange with both homologous and mismatched substrates, that is, close to the levels observed for *Sc*Dmc1 (Fig. 4*D*). Compared to *Sc*Rad51, *Tr*Rad51 possesses greater tolerance of mismatched pairing (87% in *Tr*Rad51 vs. 52% in *Sc*Rad51) during strand exchange (Fig. 4*E*). Thus, *Tr*Rad51, like *Sc*Dmc1, has an intrinsic property to harbor a better mismatch tolerance ability than *Sc*Rad51.

***Tr*Rad51 Stabilizes Triplex-State DNA Containing Mismatch Sequence.** To investigate if *Tr*Rad51 can stabilize strand-exchange intermediates containing mismatched sequence, we directly measured triplex-state DNA stability using single-molecule fluorescence microscopy. In this single-molecule assay, recombinases are first assembled onto the surface-anchored, Cy5-labeled hybrid ssDNA substrate (81 nucleotides, nt) to form nucleoprotein filaments (Fig. 5*A*). Next, 40-bp-long Cy3-labeled dsDNA containing 15-nt homologous sequence (or containing one mismatch sequence at the 11th nt position) was introduced to the reaction chamber to induce formation of the triplex strand-exchanged state. After 10 min, unbound Cy3-labeled dsDNA molecules were washed away, and disappearance of colocalized

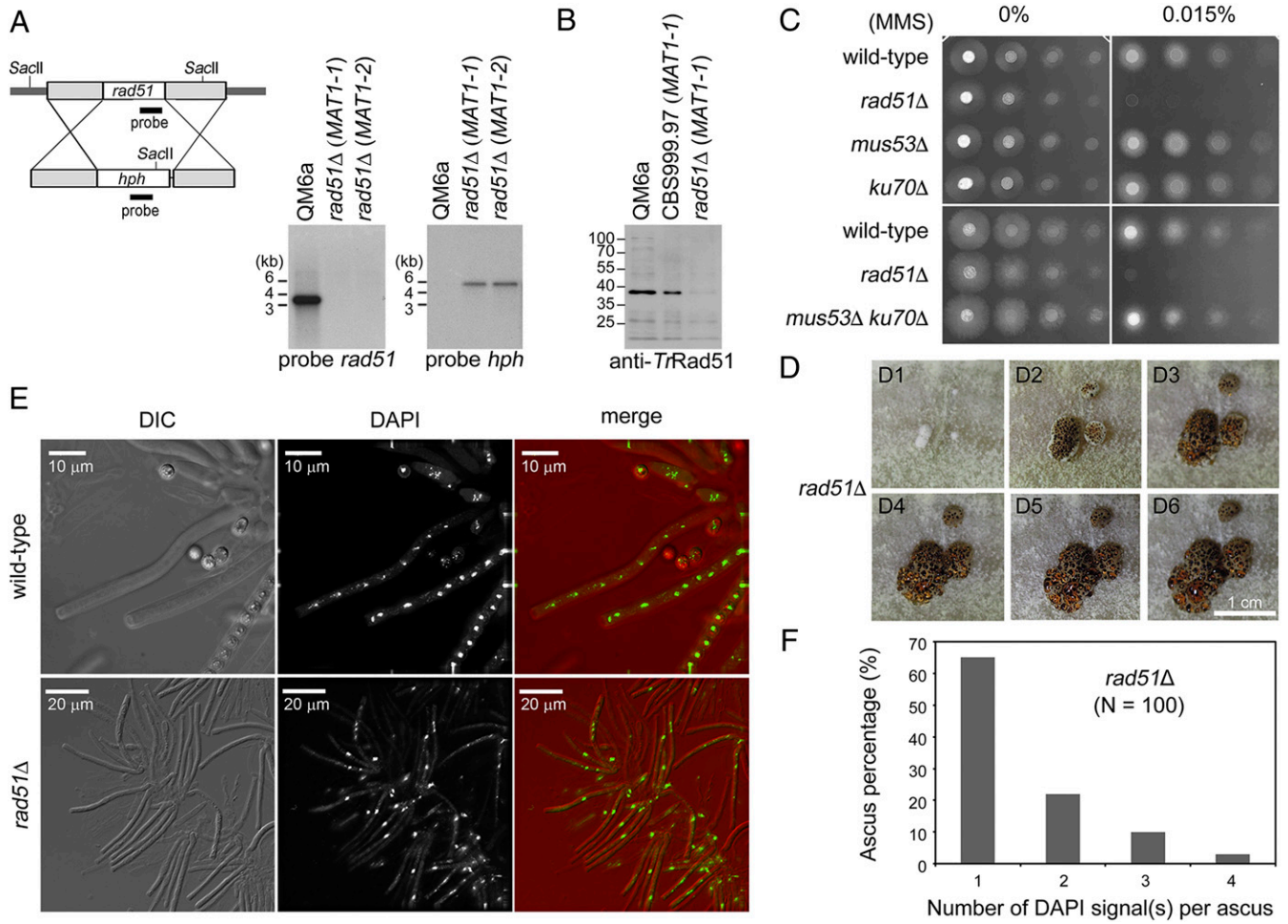

Fig. 3. *Tr*Rad51 is essential for DSB repair during vegetative growth and meiosis. (*A*) Generation of *T. reesei rad51*Δ mutants. The cassettes for removal of *rad51*. The protein-encoding regions and the hygromycin selectable marker (*hph*) are indicated. Shaded boxes represent the upstream and downstream sequences of the protein-encoding genes. The restriction enzyme sites are indicated by italics. The three DNA probes for Southern hybridization are indicated by black boxes. For Southern hybridization, genomic DNA was isolated, digested by the indicated restriction enzyme(s), and then visualized by Southern blotting. (*B*) Western blot analysis. Total cell lysate of indicated *T. reesei* haploid strains was prepared by using the trichloroacetic acid precipitation protocol we developed previously (39). Total proteins were separated by sodium dodecyl sulfate polyacrylamide gel electrophoresis. Anti-*Tr*Rad51 monoclonal antibodies were used to visualize *Tr*Rad51 proteins by Western blotting. (*C*) MMS resistance. Spot assay showing fivefold serial dilutions of indicated conidia (asexual spores) grown on MEA plates with no or 0.015% (wt/vol) MMS. (*D*) *Tr*Rad51 is dispensable for the formation of stromata. Photographs of representative developing *rad51*Δ homozygous stromata at indicated day (*D*) after induction of sexual development. (*E*) Visualization of asci from WT and *rad51*Δ homozygous zygotes. Rosettes of asci were dissected from developing fruiting bodies ($n > 10$), stained with 4′,6-diamidino-2-phenylindole (DAPI), and then visualized by fluorescence microscopy. Representative differential interference contrast (DIC) and DAPI fluorescent images are shown. (*F*) Percentage of *rad51*Δ asci with one, two, three, or four DAPI fluorescent spots.

Cy3-dsDNA/Cy5-nucleoprotein filaments directly represents dissociation of the triplex state (Fig. 5*A*). By assessing levels of the triplex state at different time points, we could determine the dissociation rate and, thus, stability of the triplex state. We compared dissociation rates of the triplex state of DNA substrates containing either 15-nt full homology or one mismatched base pair. Dissociation rates of *Sc*Dmc1 were similar for DNA substrates with or without mismatch (Fig. 5*B*), suggesting that *Sc*Dmc1 can stabilize such mismatches, consistent with the previous reports (7, 43). As a control, we used DNA substrates containing only 12-nt full homology and observed faster dissociation than for 15-nt full homology (Fig. 5*B*). In the case of *Sc*Rad51, the dissociation rate of triplex DNA substrate with a mismatch was much higher than for that with 15-nt full homology, indicating that *Sc*Rad51 cannot effectively stabilize the mismatched base pair (Fig. 5*C*). In the case of *Tr*Rad51, the dissociation rate of the triplex DNA substrate containing one mismatch was similar to that of the triplex DNA substrate with full homology (Fig. 5*D* and *SI Appendix*, Table S17). Therefore, *Tr*Rad51 behaves more similarly to *Sc*Dmc1, and both have better mismatch tolerance than *Sc*Rad51. As *Tr*Rad51 is able to stabilize the mismatched triplex state during D-loop formation to the same extent as *Sc*Dmc1, *Tr*Rad51 can efficiently catalyze strand exchange with mismatched substrates, consistent with the findings of our fluorescence-based strand exchange assay (Fig. 4).

Identification of Amino Acid Residues in *Tr*Rad51 Responsible for Mismatch Tolerance during Meiotic Recombination. It has recently been demonstrated that *Sc*Dmc1 possesses better mismatch tolerance than *Sc*Rad51 through three key L1 amino acids that are conserved only within the Dmc1 lineage of the recombinase family (43). Importantly, a chimeric *Sc*Rad51 mutant, in which *Sc*Rad51 lineage-specific amino acids were swapped with their

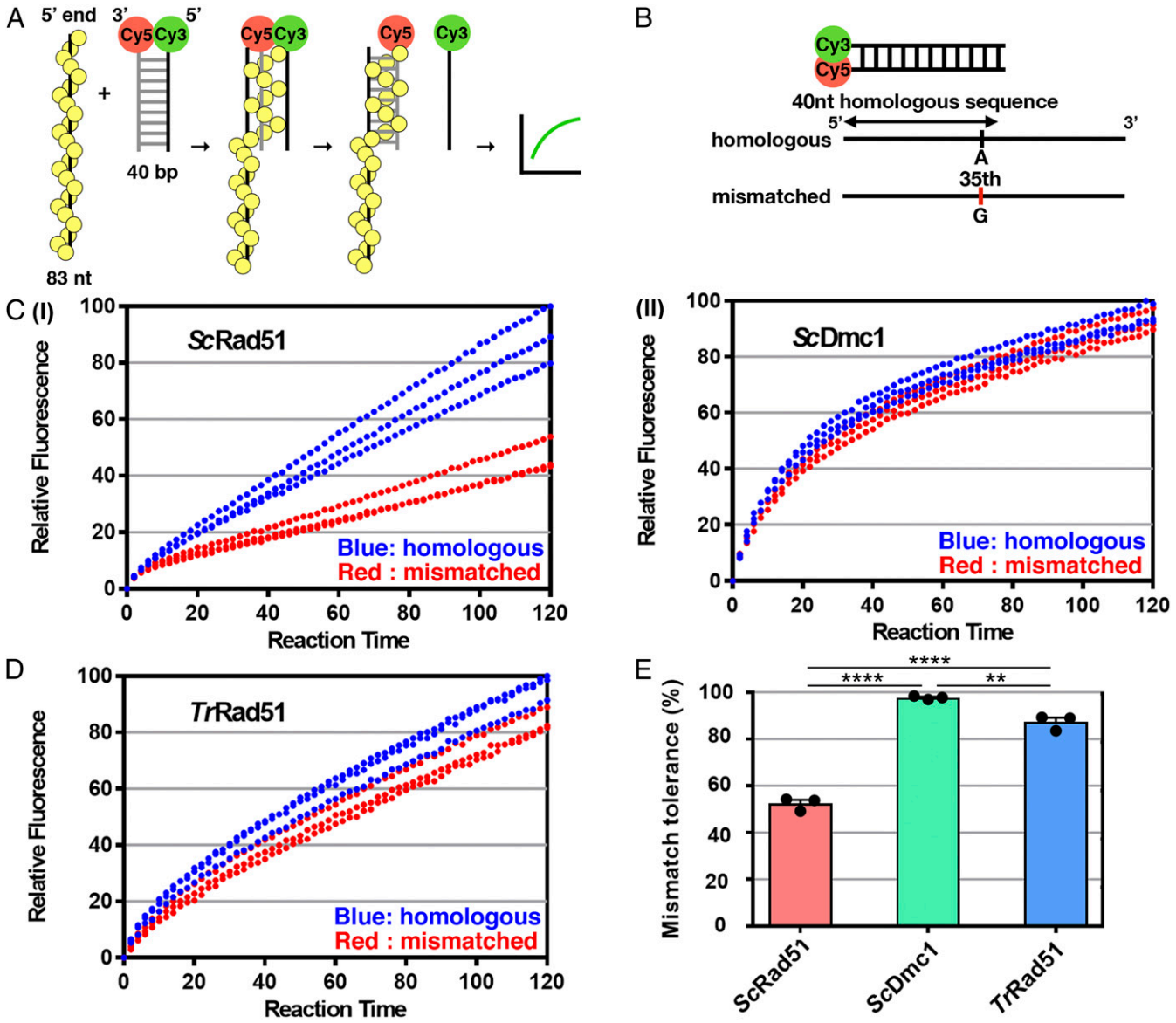

Fig. 4. *Tr*Rad51 can process strand exchange with mismatched substrate. Fluorescence-based strand-exchange assay reveals a better mismatch tolerance of *Tr*Rad51 for mismatched substrate in strand exchange compared to *Sc*Rad51. (*A*) Schematic of the fluorescence-based strand-exchange assay. Successful strand-exchange events separate two fluorophores, resulting in increased Cy3 signal (see *SI Appendix, Materials and Methods*). (*B*) Schematics of homologous and mismatched substrates. (*C*) *Sc*Rad51 (I)- or *Sc*Dmc1 (II)-mediated strand exchange with homologous (blue) or mismatched (red) substrates was monitored by Cy3 emission signal at the indicated reaction time. Experimental repeats are presented as dotted curves and statistical analysis of all repeats is reported in E. (*D*) *Tr*Rad51-mediated strand exchange with all substrates was monitored by Cy3 emission signal at the indicated reaction time. (*E*) The mismatch tolerances of all recombinases with mismatched/homologous substrates were determined at 120 min. $^{**}P < 0.01$; $^{****}P < 0.0001$. Data shown are average values ± SEM from three independent experiments. Statistics was performed by one-way ANOVA with Tukey's post hoc test.

lineage-specific counterparts from *Sc*Dmc1, regained the ability to stabilize heteroduplex DNA joints with mismatched triplets. Consistent with this notion, *C. elegans* RAD-51 (*Ce*RAD-51), a Rad51-only species, harbors amino acids that very closely resemble the three conserved in Dmc1. Moreover, mutation of those canonical Dmc1 amino acids in *Ce*RAD-51 results in attenuation of mismatch stabilization and severe meiotic defects due to the generation of toxic recombination intermediates (43). Through primary structure alignment (Fig. 6*A*), we found that those three conserved amino acids are not preserved in the Rad51 proteins of Rad51-only filamentous fungi, including *Tr*Rad51. A few amino acid residues in the middle of L2 also differ among the Rad51 proteins of "dual-RecA" and "Rad51-only" eukaryotes (Fig. 6*A*).

Next, we generated yeast S288c/SK1 hybrid diploid strains expressing chimeric *Sc*Rad51 protein harboring *Tr*Rad51 L1- and/or L2-specific amino acids (*SI Appendix*, Table S18). The *Sc*Rad51-*Tr*L1 mutant protein hosts three amino acid substitutions (S291T, A298N, and M301T), whereas two *Sc*Rad51 amino acid residues (M335 and A336) have been replaced by four *Tr*Rad51 amino acid residues (i.e., PSAM) in the *Sc*Rad51-*Tr*L2 mutant protein (Fig. 6*B*). The *Sc*Rad51-*Tr*L1L2 chimeric mutant protein hosted both of these latter mutations (Fig. 6*B*). Western blot analysis confirmed that all three of these chimeric mutant proteins were expressed (*SI Appendix*, Fig. S18). We also observed that the corresponding three chimeric mutant lines could support normal vegetative growth on yeast extract–peptone–dextrose (YPD) plates (complete media) containing no or 0.01%

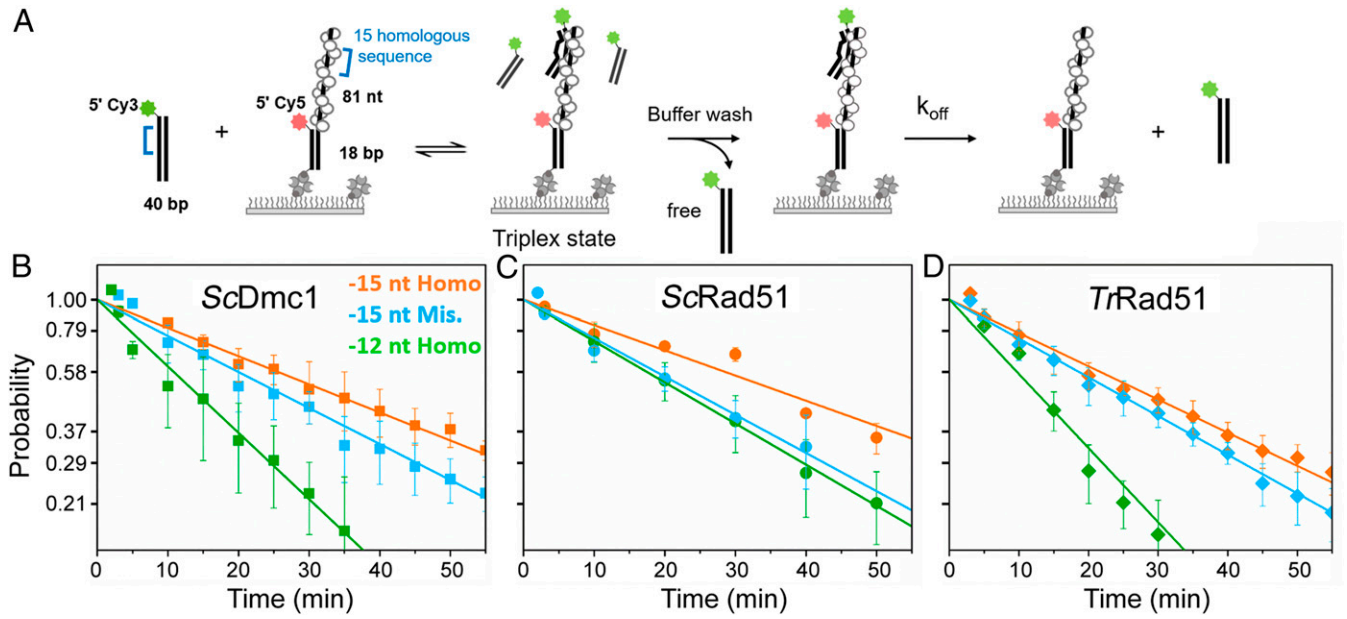

Fig. 5. *Tr*Rad51 stabilizes mismatched triplex-state DNA. Single-molecule triplex-state stability experiments reveal similar stabilities of *Tr*Rad51 on sequences with full homology and sequences containing mismatched DNA. (*A*) Schematic of single-molecule triplex-state stability experiment. (*B–D*) Kinetics of triplex-state dissociation of 15-nt full homologous (in orange), 15-nt containing one mismatched sequence (in blue), and 12-nt full homology DNA substrates (in green) measured for *Sc*Dmc1 (*B*), *Sc*Rad51 (*C*), and *Tr*Rad51 (*D*), respectively. The proportions of triplex state DNA are plotted in natural log-scale, and the slope of the plot represents the dissociation rate. Error bars represent the SEM of three replicates. The dissociation rates are listed in *SI Appendix*, Table S17.

MMS (Fig. 6*C*). Intriguingly, the *rad51-trL1* and *rad51-trL1L2* mutant lines showed slightly lower viability than WT and *rad51-trL2* on YPD plates with 0.02% MMS (Fig. 6*C*). Accordingly, the order of MMS resistance during vegetative growth was WT ≈ *rad51-trL2* > *rad51-trL1* ≈ *rad51-trL1L2*. Similarly, in *DMC1 HED1* S288c/SK1 hybrid diploid cells, these three chimeric mutant lines can support normal sporulation. The order of their capability to produce viable spores (i.e., spore viability) is WT (84%) > *rad51-trL2* (79%) > *rad51-trL1* (51%) ≈ *rad51-trL1L2* (53%) (Fig. 6*D*). We also determined if S288c/SK1 *dmc1*Δ *hed1*Δ diploid cells expressing these three mutant proteins could support sporulation and the formation of viable spores. We found that S288c/SK1 *dmc1*Δ *hed1*Δ diploid cells expressing *Sc*Rad51-*Tr*L2 produced more viable spores (spore viability = 24%, $P = 0.018$) than those expressing WT *Sc*Rad51 (spore viability = 15%) (Fig. 6*D*). S288c/SK1 *dmc1*Δ *hed1*Δ diploid cells expressing *Sc*Rad51-*Tr*L1 failed to undergo the first meiotic nuclear division (MI) and did not generate dyads, triads, or tetrads. Interestingly, S288c/SK1 *dmc1*Δ *hed1*Δ diploid cells expressing *Sc*Rad51-*Tr*L1L2 produced as many viable spores (spore viability = 16%) as the S288c/SK1 *dmc1*Δ *hed1*Δ diploid cells did (spore viability = 15%) (Fig. 6*D*). Based on these data, we infer that *Tr*Rad51 and *Sc*Rad51 underwent parallel changes in L1 and L2 during evolution to retain optimal capacity to catalyze HR. Notably, these parallel changes in L1 and L2 are more critical for repairing Spo11-induced DSBs during hybrid meiosis than for repairing MMS-induced DNA damage during vegetative growth.

It was previously reported that *Sc*Rad51^{M301Q} could stabilize mismatched HR intermediates in vitro and support a higher recombination frequency for mismatched substrates during vegetative growth in vivo (43). We also generated a series of S288c/SK1 *dmc1*Δ *hed1*Δ diploid cells expressing different *Sc*Rad51 mutant proteins, that is, *Sc*Rad51^{S291T}, *Sc*Rad51^{S291T}-*Tr*L2, *Sc*Rad51^{A298N}, *Sc*Rad51^{A298N}-*Tr*L2, *Sc*Rad51^{M301T}, *Sc*Rad51^{M301T}-*Tr*L2, *Sc*Rad51^{M301Q}, and *Sc*Rad51^{M301Q}-*Tr*L2. We found that all of these S288c/SK1 *dmc1*Δ *hed1*Δ diploid cells produced more viable spores (spore viability = 24 to 45%) than those expressing WT *Sc*Rad51 (15%), *Sc*Rad51-*Tr*L2 (24%), or *Sc*Rad51-*Tr*L1L2 (16%) (Fig. 6*D*). These results indicate that each of the three amino acid substitutions (S291, A298, and M301) in *Sc*Rad51 can enhance (at least partly) the capacity of *Sc*Rad51 to catalyze interhomolog recombination during meiosis of S288c/SK1 hybrid diploid cells. However, this function of *Sc*Rad51 is undermined by the A298N point mutation or, more severely, by simultaneous substitution of all three L1-specific amino acids. Interestingly, parallel changes in L2 could restore the corresponding function of *Sc*Rad51^{A298N} and *Sc*Rad51-*Tr*L1 in meiosis (Fig. 6*D*).

Discussion

In this study, we have first demonstrated that *T. reesei* is a Rad51-only organism. In a homozygous *rad51*Δ cross, perithecia matured to full size and asci developed to full size. However, those asci were abortive, arresting either before (~65%) or during (~35%) meiotic nuclear divisions and eventually yielding no mature ascospores. Interestingly, *N. crassa* meiotic mutant *mei-3* (*rad51*) exhibited an almost identical meiotic arrest phenotype (44). We infer that the meiotic cell-cycle arrest phenotype of *T. reesei rad51*Δ is similar to those of *S. cerevisiae rad51*Δ or *dmc1*Δ lines (45) in which unrepaired DSBs accumulate, leading to activation of Mec1^{ATR} and Tel1^{ATM}, two evolutionarily conserved DNA damage checkpoint kinases (46, 47). *S. cerevisiae dmc1*Δ or *rad51*Δ *dmc1*Δ lines display a strong meiotic prophase arrest phenotype (45). In contrast, *S. cerevisiae rad51*Δ mutants display a less uniform meiotic progression defect than *S. cerevisiae dmc1* mutants. Although MI is delayed in *S. cerevisiae rad51*Δ, a fraction of the culture goes on to execute MI (48). Consistent with our supposition, we found that the near-complete genome sequences of QM6a (18), CBS999.97(*MAT1-1*), and CBS999.97(*MAT1-2*) (this study) all encode orthologs of Mec1^{ATR} and Tel^{ATM}.

Genomics and single-molecule analyses have clearly demonstrated that Dmc1 possesses a better mismatch tolerance than its Rad51 counterpart during meiotic interhomolog recombination in the "dual-RecA" eukaryotes (6, 7, 9–11). Consistent with this notion, our fluorescence-based strand exchange assay confirmed

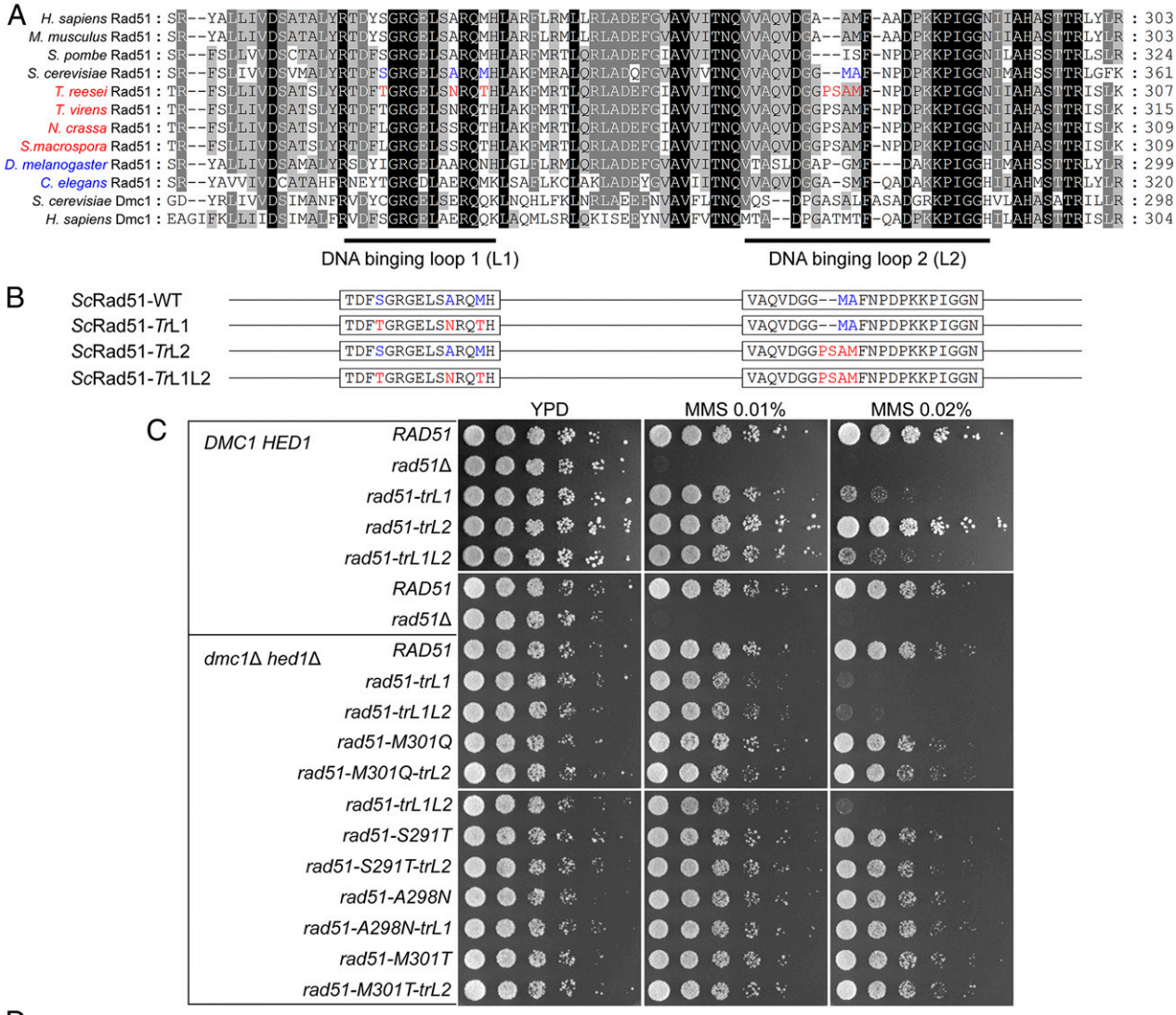

D

SK1/S288c hybrid diploid	Spore viability (%)	*n* of dissected spores	SK1/S288c hybrid diploid	Spore viability (%)	*n* of dissected spores
RAD51	84	288	*RAD51 dmc1Δ hed1Δ*	15	216
rad51-trL1	51 ***	216	*rad51-trL1 dmc1Δ hed1Δ*	no spore	n.d.
rad51-trL2	79	216	*rad51-trL2 dmc1Δ hed1Δ*	24 *	216
rad51-trL1L2	53 ***	212	*rad51-trL1L2 dmc1Δ hed1Δ*	16	168
rad51-S291T	87	216	*rad51-S291T dmc1Δ hed1Δ*	32 ***	212
rad51-S291T-trL2	83	216	*rad51-S291T-trL2 dmc1Δ hed1Δ*	39 ***	216
rad51-A298N	89	216	*rad51-A298N dmc1Δ hed1Δ*	24 *	144
rad51-A298N-trL2	88	216	*rad51-A298N-trL2 dmc1Δ hed1Δ*	36 ***	216
rad51-M301T	85	212	*rad51-M301T dmc1Δ hed1Δ*	45 ***	216
rad51-M301T-trL2	90	216	*rad51-M301T-trL2 dmc1Δ hed1Δ*	41 ***	216
rad51-M301Q	88	216	*rad51-M301Q dmc1Δ hed1Δ*	31 ***	216
rad51-M301Q-trL2	88	216	*rad51-M301Q-trL2 dmc1Δ hed1Δ*	36 ***	212

Fig. 6. Chimeric *Sc*Rad51 with *Tr*Rad51 L2-specific amino acids can partially rescue the low spore viability phenotype of S288c/SK1 *dmc1*Δ *hed1*Δ hybrid diploid cells. (*A*) Comparison of Rad51 L1 and L2 amino acid sequences from "dual-RecA" and "Rad51-only" sexual eukaryotes. Species names in red indicate "Rad51-only" Pezizomycotina filamentous fungi; species names in blue indicate "Rad51-only" animals. L1/L2 amino acids that are *Sc*Rad51-specific and *Tr*Rad51-specific are highlighted in blue and red, respectively. Yeast and human Dmc1 were added to the alignment to aid comparison. Amino acids that are completely or partially conserved in these recombinase proteins are shaded in black or gray, respectively. (*B*) Schematic representation of *S. cerevisiae* mutant Rad51 proteins (*Sc*Rad51) carrying amino acid substitutions derived from *T. reesei* L1 (*Tr*L1) and/or L2 (*Tr*L2). Amino acids marked in red and blue represent residues with or without substitutions, respectively (*SI Appendix*, Table S18). (*C*) MMS resistance. Spot assay showing fivefold serial dilutions of indicated strains grown on YPD plates with 0, 0.01%, or 0.02% MMS. (*D*) Spore viability. Spore viability of indicated S288c/SK1 hybrid diploid cells was analyzed after 3 d on sporulation media at 30 °C. To score spore viability, only tetrads (but not dyads or triads) were dissected on YPD. Asterisks indicate spore viability of the *rad51* mutants that is significantly different from that of WT under the same genetic background with *P* values calculated using *Z*-tests of two proportions (*$P < .05$ and ***$P < .001$). n.d. (not determined)

that *Sc*Dmc1 possesses better mismatch tolerance than *Sc*Rad51 (100% vs. 53%). It is worth noting that *Tr*Rad51 exhibited a slight decrease in mismatched strand-exchange activity to 87% in comparison with *Sc*Dmc1 (100%). Our genomic analyses also reveal that mismatch tolerance in QM6a/CBS999.97(*MAT1*-1) hybrid meiosis is ≥3.6-fold higher than that of SK1/S288c *dmc1*Δ *hed1*Δ hybrid meiosis (Fig. 2 and *SI Appendix*, Table S15). Accordingly, we suggest that *Tr*Rad51 is better than *Sc*Rad51 in tolerating mismatched sequences during meiotic interhomolog recombination. This hypothesis is also consistent with the finding of higher sequence heterogeneity between QM6a and CBS999.97(*MAT1-1*) than between S288c and SK1, regardless of whether all "unalignable" or "strain-specific" sequences in both hybrid diploids are included or excluded for the estimation of genome-wide sequence heterogeneity (Dataset S1).

The findings of this study and those of others (43) strongly indicate that ancestral Rad51 proteins of "Rad51-only" species underwent convergent evolution to acquire Dmc1-like activities. A previous study using chimeric *Sc*Rad51 mutants showed that structural variation (i.e., *Sc*Rad51-M301) in L1 is critical for endowing mismatch tolerance (43). In contrast, our comparative analyses of *Sc*Rad51 and *Tr*Rad51 have revealed further insights regarding capacities for mismatch tolerance. First, we have identified three additional L1 amino acid substitutions (i.e., S291T, A298N, and M301T) that promote the mismatch tolerance of *Sc*Rad51 in vivo. We infer that the L1 region of *Tr*Rad51, like those in *Sc*Dmc11 and *Ce*Rad51 (43), is critical for their capacity to tolerate mismatched sequences during homology searching. Second, we show that simultaneous replacement of all three of these critical amino acids (S291, A298, and M301) in *Sc*Rad51-L1 with those of *Tr*Rad51-L1 has a much stronger inhibitory effect on meiotic recombination in SK1/S288c hybrid diploid cells than MMS-induced DNA damage repair during vegetative growth. Interestingly, a parallel change in *Sc*Rad51-L2 can specifically rescue this L1-mediated inhibition on meiosis but not vegetative growth (Fig. 6). Thus, L1 and L2 apparently act together (at least for *Tr*Rad51) to acquire mismatch tolerance during homology searching. This notion is consistent with two previous structural biology studies in which human RAD51 and *E. coli* RecA were reported to utilize L1 and L2 to catalyze ssDNA–dsDNA interactions and DNA strand exchange (49, 50).

Since all of the mutations we analyzed here could not completely restore *Sc*Rad51 functions during both vegetative growth and hybrid meiosis (even in the presence of Dmc1 and Hed1), other structural variants in *Tr*Rad51 and/or *Tr*Rad51 accessory factors might also be involved in regulating mismatch tolerance in vivo. Further structural and functional studies on *Tr*Rad51 and its accessory factors will elucidate the mechanisms underlying mismatch tolerance in *T. reesei*.

In conclusion, we show here that hybrid crosses of QM6a and CBS999.97(*MAT1-1*) are an ideal model for studying the molecular mechanism of Rad51-only meiosis. Given the availability of near-complete genome sequences and a newly invented bioinformatics tool (TSETA) (31), this model is also suitable for revealing novel insights into other fundamental questions in biology (e.g., RIP and RIP-associated DNA methylation), and it may have potential economic applications (e.g., improvement of industrial strains).

Materials and Methods

All materials and methods are provided in *SI Appendix*, including miscellaneous, pulsed-field gel electrophoresis, cytology, PacBio genome sequence and assembly, NGS-based SNP calling, assembly of NGS-based genome sequences of 16 F1 progeny, protein expression plasmids, protein purification, DNA substrates, biochemical assays, and single-molecule biophysical assays and yeast strains.

Data Availability. The complete genome sequences and raw datasets have been deposited in the National Center for Biotechnology Information, https://www.ncbi.nlm.nih.gov/bioproject/ (accession nos. PRJNA325840, PRJNA352653, PRJNA386077, PRJNA382020, and 433292 (*SI Appendix*, Table S1). All study data are included in the article, *SI Appendix*, and Datasets S1 and S2.

ACKNOWLEDGMENTS. This work was supported by Academia Sinica, Taiwan, Republic of China (AS-105-TP-B07 and AS108-TP-B07 to H.-W.L., P.C. and T.-F.W. and postdoctoral fellowships to Y.-C.C. and T.-T.W.) and the Ministry of Science and Technology, Taiwan, Republic of China (MOST 163-2311-B-001-016-MY3 to T.-F.W., MOST 105-2314-B-002-073-MY4 to P.C., and MOST 107-2113-M-002-010-MY3 to H.-W.L.). We thank Shu-Yun Tung (IMB Genomics Core) for NGS sequencing service, Kun-Hai Ye and Yi-Ning Chen (IMB Bioinformatics Core) for statistical help and bioinformatics consulting service, John O'Brien for English editing, Chin-Fu Cheng and John Kung (IMB Animal Facility) for programming help with the bioinformatics studies, and Yu-Tang Huang (IMB Computer Room) for maintaining the computer workstation.

1. N. Kleckner, Meiosis: How could it work? *Proc. Natl. Acad. Sci. U.S.A.* **93**, 8167–8174 (1996).
2. T. Allers, M. Lichten, Differential timing and control of noncrossover and crossover recombination during meiosis. *Cell* **106**, 47–57 (2001).
3. G. V. Börner, N. Kleckner, N. Hunter, Crossover/noncrossover differentiation, synaptonemal complex formation, and regulatory surveillance at the leptotene/zygotene transition of meiosis. *Cell* **117**, 29–45 (2004).
4. N. Hunter, Meiotic recombination: The essence of heredity. *Cold Spring Harb. Perspect. Biol.* **7**, a016618 (2015).
5. M. S. Brown, D. K. Bishop, DNA strand exchange and RecA homologs in meiosis. *Cold Spring Harb. Perspect. Biol.* **7**, a016659 (2014).
6. J. P. Lao *et al*., Meiotic crossover control by concerted action of Rad51-Dmc1 in homolog template bias and robust homeostatic regulation. *PLoS Genet.* **9**, e1003978 (2013).
7. J. Y. Lee *et al*., DNA RECOMBINATION. Base triplet stepping by the Rad51/RecA family of recombinases. *Science* **349**, 977–981 (2015).
8. Z. Qi *et al*., DNA sequence alignment by microhomology sampling during homologous recombination. *Cell* **160**, 856–869 (2015).
9. M. V. Borgogno *et al*., Tolerance of DNA mismatches in Dmc1 recombinase-mediated DNA strand exchange. *J. Biol. Chem.* **291**, 4928–4938 (2016).
10. J. Y. Lee *et al*., Sequence imperfections and base triplet recognition by the Rad51/RecA family of recombinases. *J. Biol. Chem.* **292**, 11125–11135 (2017).
11. T. L. Callender *et al*., Mek1 down regulates Rad51 activity during yeast meiosis by phosphorylation of Hed1. *PLoS Genet.* **12**, e1006226 (2016).
12. M. Schmoll *et al*., The genomes of three uneven siblings: Footprints of the lifestyles of three *Trichoderma* species. *Microbiol. Mol. Biol. Rev.* **80**, 205–327 (2016).
13. V. Seidl, C. Seibel, C. P. Kubicek, M. Schmoll, Sexual development in the industrial workhorse *Trichoderma reesei*. *Proc. Natl. Acad. Sci. U.S.A.* **106**, 13909–13914 (2009).
14. C. L. Chen *et al*., Blue light acts as a double-edged sword in regulating sexual development of *Hypocrea jecorina* (*Trichoderma reesei*). *PLoS One* **7**, e44969 (2012).
15. R. Linke *et al*., Restoration of female fertility in *Trichoderma reesei* QM6a provides the basis for inbreeding in this industrial cellulase producing fungus. *Biotechnol. Biofuels* **8**, 155 (2015).
16. I. S. Druzhinina, C. P. Kubicek, Familiar stranger: Ecological genomics of the model saprotroph and industrial enzyme producer *Trichoderma reesei* breaks the stereotypes. *Adv. Appl. Microbiol.* **95**, 69–147 (2016).
17. Y. C. Chuang *et al*., *Trichoderma reesei* meiosis generates segmentally aneuploid progeny with higher xylanase-producing capability. *Biotechnol. Biofuels* **8**, 30 (2015).
18. W. C. Li *et al*., *Trichoderma reesei* complete genome sequence, repeat-induced point mutation, and partitioning of CAZyme gene clusters. *Biotechnol. Biofuels* **10**, 170 (2017).
19. B. Ewing, L. Hillier, M. C. Wendl, P. Green, Base-calling of automated sequencer traces using phred. I. Accuracy assessment. *Genome Res.* **8**, 175–185 (1998).
20. F. A. Simão, R. M. Waterhouse, P. Ioannidis, E. V. Kriventseva, E. M. Zdobnov, BUSCO: Assessing genome assembly and annotation completeness with single-copy orthologs. *Bioinformatics* **31**, 3210–3212 (2015).
21. M. Seppey, M. Manni, E. M. Zdobnov, BUSCO: Assessing genome assembly and annotation Completeness. *Methods Mol. Biol.* **1962**, 227–245 (2019).
22. E. V. Kriventseva *et al*., OrthoDB v10: Sampling the diversity of animal, plant, fungal, protist, bacterial and viral genomes for evolutionary and functional annotations of orthologs. *Nucleic Acids Res.* **47**, D807–D811 (2019).
23. J. Palmer, Funannotate: Fungal genome annotation scripts. GitHub. https://github.com/nextgenusfs/funannotate. Accessed 2 January 2021.
24. R. Aramayo, E. U. Selker, *Neurospora crassa*, a model system for epigenetics research. *Cold Spring Harb. Perspect. Biol.* **5**, a017921 (2013).
25. E. Gladyshev, Repeat-induced point mutation and other genome defense mechanisms in Fungi. *Microbiol. Spectr.* **5**, 5 (2017).
26. W. C. Li, C. L. Chen, T. F. Wang, Repeat-induced point (RIP) mutation in the industrial workhorse fungus *Trichoderma reesei*. *Appl. Microbiol. Biotechnol.* **102**, 1567–1574 (2018).

27. C. L. Schardl *et al*., Plant-symbiotic fungi as chemical engineers: Multi-genome analysis of the clavicipitaceae reveals dynamics of alkaloid loci. *PLoS Genet.* **9**, e1003323 (2013).
28. D. J. Winter *et al*., Repeat elements organise 3D genome structure and mediate transcription in the filamentous fungus *Epichloë festucae*. *PLoS Genet.* **14**, e1007467 (2018).
29. G. Marçais *et al*., MUMmer4: A fast and versatile genome alignment system. *PLOS Comput. Biol.* **14**, e1005944 (2018).
30. D. Shigemizu *et al*., IMSindel: An accurate intermediate-size indel detection tool incorporating de novo assembly and gapped global-local alignment with split read analysis. *Sci. Rep.* **8**, 5608 (2018).
31. W. C. Li, H. C. Liu, Y. J. Lin, S. Y. Tung, T. F. Wang, Third-generation sequencing-based mapping and visualization of single nucleotide polymorphism, meiotic recombination, illegitimate mutation and repeat-induced point mutation. *NAR Genomics Bioinformatics* **2**, lqaa056 (2020).
32. C. M. Anderson *et al*., ReCombine: A suite of programs for detection and analysis of meiotic recombination in whole-genome datasets. *PLoS One* **6**, e25509 (2011).
33. A. Oke, C. M. Anderson, P. Yam, J. C. Fung, Controlling meiotic recombinational repair - specifying the roles of ZMMs, Sgs1 and Mus81/Mms4 in crossover formation. *PLoS Genet.* **10**, e1004690 (2014).
34. E. A. Winzeler *et al*., Direct allelic variation scanning of the yeast genome. *Science* **281**, 1194–1197 (1998).
35. E. Mancera, R. Bourgon, A. Brozzi, W. Huber, L. M. Steinmetz, High-resolution mapping of meiotic crossovers and non-crossovers in yeast. *Nature* **454**, 479–485 (2008).
36. W. C. Li *et al*., Two different pathways for initiation of Trichoderma reesei Rad51-only meiotic recombination. *bioRxiv* [Preprint] (2019). https://doi.org/10.1101/644443 (Accessed 21 May 2019).
37. L. A. Pray, DNA replication and causes of mutation. *Nat. Educ.* **1**, 214 (2008).
38. C. D. Lee *et al*., An improved SUMO fusion protein system for effective production of native proteins. *Protein Sci.* **17**, 1241–1248 (2008).
39. C. H. Cheng *et al*., SUMO modifications control assembly of synaptonemal complex and polycomplex in meiosis *of Saccharomyces cerevisiae*. *Genes Dev.* **20**, 2067–2081 (2006).
40. Z. Guangtao *et al*., Gene targeting in a nonhomologous end joining deficient *Hypocrea jecorina*. *J. Biotechnol.* **139**, 146–151 (2009).
41. M. G. Steiger *et al*., Transformation system for *Hypocrea jecorina* (*Trichoderma reesei*) that favors homologous integration and employs reusable bidirectionally selectable markers. *Appl. Environ. Microbiol.* **77**, 114–121 (2011).
42. K. Ito, B. Argunhan, H. Tsubouchi, H. Iwasaki, Real-time observation of the DNA strand exchange reaction mediated by Rad51. *J. Vis. Exp.*, 10.3791/59073 (2019).
43. J. B. Steinfeld *et al*., Defining the influence of Rad51 and Dmc1 lineage-specific amino acids on genetic recombination. *Genes Dev.* **33**, 1191–1207 (2019).
44. N. B. Raju, D. D. Perkins, Barren perithecia in *Neurospora crassa*. *Can. J. Genet. Cytol.* **20**, 41–59 (1978).
45. D. K. Bishop, D. Park, L. Xu, N. Kleckner, *DMC1*: A meiosis-specific yeast homolog of E. coli recA required for recombination, synaptonemal complex formation, and cell cycle progression. *Cell* **69**, 439–456 (1992).
46. D. Lydall, Y. Nikolsky, D. K. Bishop, T. Weinert, A meiotic recombination checkpoint controlled by mitotic checkpoint genes. *Nature* **383**, 840–843 (1996).
47. J. C. Mallory, T. D. Petes, Protein kinase activity of Tel1p and Mec1p, two *Saccharomyces cerevisiae* proteins related to the human ATM protein kinase. *Proc. Natl. Acad. Sci. U.S.A.* **97**, 13749–13754 (2000).
48. A. Shinohara, S. Gasior, T. Ogawa, N. Kleckner, D. K. Bishop, *Saccharomyces cerevisiae recA* homologues *RAD51* and *DMC1* have both distinct and overlapping roles in meiotic recombination. *Genes Cells* **2**, 615–629 (1997).
49. Z. Chen, H. Yang, N. P. Pavletich, Mechanism of homologous recombination from the RecA-ssDNA/dsDNA structures. *Nature* **453**, 489–494 (2008).
50. J. Xu *et al*., Cryo-EM structures of human RAD51 recombinase filaments during catalysis of DNA-strand exchange. *Nat. Struct. Mol. Biol.* **24**, 40–46 (2017).